

Increasing the Aerodynamic Performance of a Small Fixed-Wing UAV Using Passive Bio-inspired Microfibers

Dioser Santos and Victor Maldonado*†*

** Texas Tech University, Lubbock, TX, 79409 USA*

dioser.santos@ttu.edu – victor.maldonado@ttu.edu

† Corresponding Author

Abstract

Bio-inspired microfibers are applied to the suction wing surface of a small flying wing UAV and their effect on aerodynamics and control surface performance is analyzed via wind tunnel experiments. The effects of fiber height, coverage area, flow regime and angle of attack are studied in the use of microfibers as a passive flow control method. Taller microfibers, when compared to a smooth wing, provide a drag reduction of up to 24.7% for $C_L = 0.9$ at higher Reynolds number, whereas shorter fibers perform better at lower Reynolds, with a 24.2% drag reduction for the same lift coefficient. Control surface testing shows that when applying microfibers to the elevon and its upstream wing region, there is an improvement in pitch moment authority at higher angles of attack, with an increase in the pitch coefficient magnitude of up to 22.4%. Microfiber coating films, while being incredibly practical for use, have the potential to improve the performance of small flying vehicles in certain conditions.

1. Introduction

Passive flow control techniques of diverse natures are commonly used in fixed-wing aircraft to enhance aerodynamic efficiency by delaying flow separation or to mitigate undesirable stall behavior. Vortex generators, wing fences, notches and strakes are some flow control methods commonly employed in conventional aircraft [1], [2]. For these high Reynolds number applications, the turbulent boundary layer has greater resistance to separation, which results in better aerodynamic performance [3]. In the case of small unmanned aerial vehicles (UAV), operation usually occurs at low or transitional Reynolds number range, where laminar separation can occur, increasing pressure drag significantly. The use of passive flow control has the potential to provide great improvements in performance by causing the flow to transition early, therefore delaying separation and reducing pressure drag as a consequence [4]. Some examples of enhancement techniques are the use of vortex generators, bumps, trips or roughness elements [5–8]

In recent years, more attention has been given to bio-inspired surfaces in aerodynamic or hydrodynamic applications, primarily involving features observed on the skin of marine mammals, fish, unique bird feathers [9], or flight techniques inspired by insects and bats [10–12]. The use of protrusions that resemble the tubercles found on humpback whale flippers has been studied by [13–15], to satisfactory performance improvements. Ridges mimicking the ones found on fish skin have been analyzed in experimental and computational studies, showing that small surface features can improve aerodynamic performance of small wings and delay stall similarly to vortex generators, and increase L/D ratio at low angles of attack [16–20]. Along the same lines, micrometric structures found on shark skin called denticles (Fig. 1 a) have been analyzed and determined to reduce pressure drag by keeping the flow attached for longer [21–27]. In this study, similar structures in the form of bio-inspired microfibers in gecko feet called ‘setae’ (Fig. 1b and c) are used on the surface of a small fixed-wing UAV and their performance is evaluated experimentally via wind tunnel testing. In an experimental study, these bio-inspired microfibers have been shown to reduce flow separation by re-energizing the boundary layer due to pressure modulations at the surface of microfibers leading to smaller flow re-circulation areas in

DOI: ADD DOINUMBER HERE

the separated region (Fig. 1d) [28, 29]. These microfibers have been shown to mitigate flow separation without the disadvantage of producing higher turbulent kinetic energy, and as a result, higher viscous losses — an issue that is present in passive flow control methods that rely on boundary layer transition. Additionally, the microfibers used in this work have an advantage over shark skin denticles in that they are manufactured onto adhesive films that can be easily applied to any smooth surface instead of being 3D printed. This avoids the limitations associated with additive manufacturing, such as increased time and cost to manufacture intricate structures.

In this research, the airplane model utilized is derived from a design called Switchblade, which is an unmanned aerial vehicle created as part of a series of reconfigurable vehicles sharing a modular platform [30]. This reconfigurability allows for various UAV versions with identical central body structures but distinct mission profiles, such as 'low-speed high endurance' (LSHE) and 'high-speed long range' (HSLR), to be prepared for flight. This study examines the application of microfibers to the UAV-HSLR variant to assess the potential for further improving its aerodynamic performance.

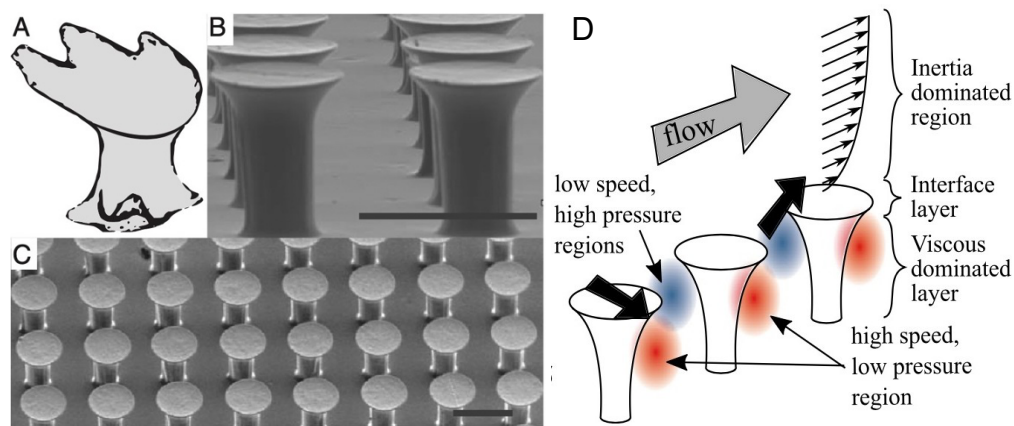


Figure 1: A) Geometry of a shark denticle, B) Side view of the bio-inspired microfibers; scale bar = 100 μm , C) Top view of an array of microfibers, and D) Pressure modulations and momentum transfer along the microfiber surface. Adapted from Bocanegra et al. [28]

2. Methodology

The Switchblade UAV consists of a tailless blended-wing-body that offers the capability of swapping wing modules for distinct mission performances. In this work, the High Speed, Long Range (HSLR) variant was used for microfiber performance testing. This aircraft is characterized by its low aspect ratio and wing area, with moderate leading edge sweep to achieve a cruise speed of Mach 0.1. The concept is shown in Figure 2 and some of its design parameters in Table 1. The balloons in the drawing show the distinct regions of the wing upper surface that were covered with microfibers. Region 1 is upstream from the control surface (Region 2), and region 3 is the remaining wing surface area up to the center body. The model was not totally covered due to difficulties in applying the adhesive film to tight corners, such as the nacelle fillets and the leading edge, although it was ensured that fibers were located upstream of the wing's maximum thickness line.

Table 1: Wing characteristics

Wing area [m ²]	Aspect ratio	Span [m]	Sweep	Taper ratio
0.324	6.3	1.43	24 ^o	0.35

The model's construction was primarily achieved through additive manufacturing, using a carbon-reinforced nylon material and finishing the surface with fine-grit sandpaper to ensure a baseline surface devoid of flaws that might impact the results. Its reconfigurable nature allows the wing module to be attached to the central section via tubular spars, enabling various wings to be tested as well, although this aspect is not investigated in the current study. The wind tunnel model is fabricated using the same techniques as a flight-worthy prototype, providing the added opportunity to assess its structural integrity under flight conditions for future research. The nacelle cover, as illustrated in Figure 3 (a), can also be detached to install a motor and propeller for propulsion test

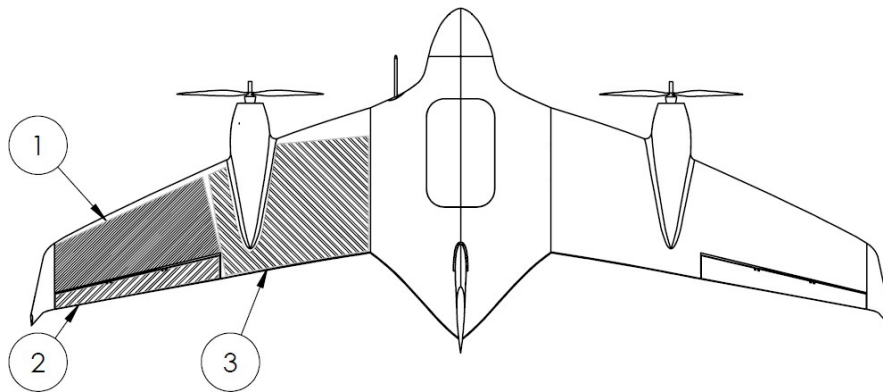


Figure 2: Top view of Switchblade small flying wing UAV

Microfibers were applied to different regions of the wing to identify potential correlation between the extent of their use and effect on aerodynamic performance. Three cases were studied: i) top of wing (all regions covered); ii) outboard, covering elevon and upstream (regions 1 and 2 only); iii) smooth wing (baseline case). For each case, two distinct free stream speeds were considered: 30 m/s and 17.3 m/s, which correspond to the aircraft cruise speed (or very close) and estimated stall speed, respectively. The different flow speeds are meant to produce distinct flow Reynolds numbers — yet consistent with the UAV operating conditions. For nomenclature purposes, the higher speed cases are referred to as “cruise Re” and lower speed, “stall Re”. The microfibers were manufactured and provided by Setex Technologies, and were studied with respect to the effect of microfiber pillar height, referring to the height of the cylindrical micro structures on the surface shown in Figure 1. The microfibers were provided in two variants with approximately 70 μm and 140 μm fiber heights.

For cases without control surface deflection, aerodynamic forces were recorded across an angle of attack range spanning from 2° to 17° . The angle was manually adjusted, and the model secured in place, with the wind tunnel switched off between tests to eliminate the influence of hysteresis or bias on the load cell. Control surface performance experiments were conducted by deflecting the elevon between -18.7° to 24.7° at three distinct angles of attack, α : 2° , 7° and 12° . It is important to note that a negative deflection angle signifies a downward movement of the elevon and an increase in the generated sectional lift. A summary of the cases can be found in Table 2.

Table 2: Experiment cases

Region	Airspeed	MAC Re	Surface	AoA	Elevon deflection	N/A
cruise	3.7×10^5		no fibers	-2° to 17°		N/A
1, 2, 3	cruise	3.7×10^5	$140\mu m$ fibers	-2° to 17°		N/A
1, 2	cruise	3.7×10^5	$140\mu m$ fibers	-2° to 17°		N/A
1, 2, 3	cruise	3.7×10^5	$70\mu m$ fibers	-2° to 17°		N/A
N/A	stall	2.1×10^5	no fibers	-2° to 17°		N/A
1, 2, 3	stall	2.1×10^5	$140\mu m$ fibers	-2° to 17°		N/A
1, 2	stall	2.1×10^5	$140\mu m$ fibers	-2° to 17°		N/A
1, 2, 3	stall	2.1×10^5	$70\mu m$ fibers	-2° to 17°		N/A
N/A	cruise	4.2×10^5	no fibers	2°	-18.7° to 24.7°	
1, 2, 3	cruise	4.2×10^5	$140\mu m$ fibers	2°	-18.7° to 24.7°	
1, 2	cruise	4.2×10^5	$140\mu m$ fibers	2°	-18.7° to 24.7°	
N/A	cruise	3.7×10^5	no fibers	7°	-18.7° to 24.7°	
1, 2, 3	cruise	3.7×10^5	$140\mu m$ fibers	7°	-18.7° to 24.7°	
1, 2	cruise	3.7×10^5	$140\mu m$ fibers	7°	-18.7° to 24.7°	
N/A	cruise	3.7×10^5	no fibers	12°	-18.7° to 24.7°	
1, 2, 3	cruise	3.7×10^5	$140\mu m$ fibers	12°	-18.7° to 24.7°	
1, 2	cruise	3.7×10^5	$140\mu m$ fibers	12°	-18.7° to 24.7°	

The experiments were conducted in the National Wind Institute (NWI) closed-loop, subsonic wind tunnel at the Reese Technology Center. The test section is 1.2 m tall and 1.8 m wide, which is large enough to accommodate the aircraft half-model in its true scale, as shown in Figure 3 (a). The half-model is attached to a circular splitter plate and the whole system is fixed to an ATI 9150 Net Gamma 6-DoF load sensor with a resolution of 0.025 N for the lift and drag forces and 0.00125 N-m for the pitching moment. Figure 3 (b) shows a schematic of the components in the system. Load cell data was acquired using a National Instruments DAQ model 6353 with a sampling rate of 1,000 Hz for 30 seconds each time. The static angles of attack were set manually using a pitch link and a digital protractor with an error of 0.1° . The setup was also equipped with a microcontroller and servo for setting the control surface at different deflection angles. Current and propeller speed (RPM) sensors, electronic speed controller (ESC), and the motor were not used in the work discussed here.

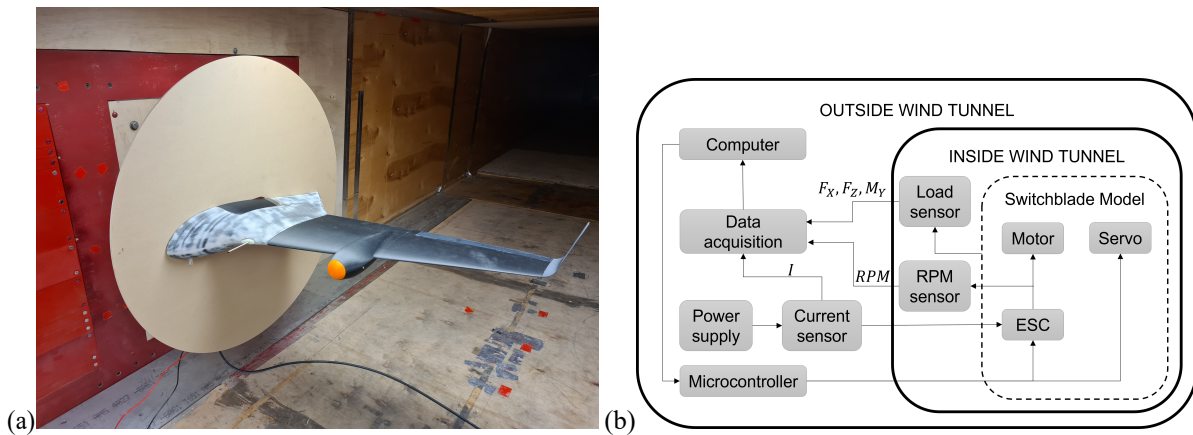


Figure 3: (a) Wind tunnel setup with HSLR variant; (b) Setup diagram

3. Results and Discussion

Aerodynamic forces and pitching moment were made dimensionless by using dynamic pressure and the reference wing area, resulting in the calculation of lift, drag, and pitching moment coefficients. Lift coefficients, drag polar and L/D ratio are shown in Figures 4 (a), (b) and (c), respectively. There was little difference between baseline and microfiber cases at the linear portion of the C_L vs. α curves, which is consistent with the expected role of the fibers; if flow separation is not prevalent, the fibers do not have much impact at increasing lift. Accordingly, there was a small gain in C_L at high angles of attack, beyond $\alpha = 10^\circ$. With the top wing surface covered with 140 μm fibers, C_L was 3.61% higher at cruise Reynolds and $\alpha = 14^\circ$. With the partially covered case, C_L was 3.89% higher in the same conditions. The 70 μm fibers on the fully covered wing lead to 3.28% increase in C_L compared to the baseline case, at $\alpha = 15^\circ$. For the stall Reynolds number cases, the increase in C_L with microfibers was less significant for both pillar heights. It is hypothesized that microfibers create a periodic, albeit weak, positive momentum transfer mechanism to the external flow, slightly raising the mean flow velocity. Additionally, the extent of flow passing over the microfibers before separation influences their capacity to postpone flow separation. A greater distance enables momentum transfer to accumulate and become effective. In this regard, passive microfibers serve as a weak and distributed flow control mechanism, while active synthetic jets, for example, act as potent yet localized flow control devices that must be positioned at or near the flow separation point to be effective.

The microfibers have a stronger effect at reducing drag, as seen in the drag polars (Fig. 4 b). At the cruise Reynolds number condition, the case with fully covered top wing surface presented a maximum drag reduction of 24.7% for $C_L = 0.90$. For the partially covered wing, drag was 23.3% lower than the baseline for the same C_L . Microfibers with 70 μm pillar height reduced the drag by 19.9%. In the stall Reynolds number condition, the maximum reduction in drag at $C_L = 0.9$ was 14.8% for the wing fully covered with 140 μm microfibers, 14.9% for the partially covered case, and 24.2% for the 70 μm fibers fully covering the wing.

The maximum aerodynamic efficiency at cruise Reynolds number is minimally affected by the use of microfibers. The greatest improvement in L/D ratio was 1.8%, in the case with 140 μm fibers partially covering the wing (Fig. 4 c). In the lower Re regime, the use of microfibers in fact reduced maximum L/D marginally. Here, the case with 140 μm fibers covering the elevon and upstream experienced a 6.9% reduction. At higher angles of attack all microfiber cases showed an increase in L/D ratio over their baselines (Fig. 4 (d)). At the cruise Reynolds number, the best performing condition is 140 μm fibers on top of the wing, with 15.3% higher L/D at $\alpha = 10^\circ$. At the stall Reynolds number, 70 μm fibers covering the top of the wing is most effective, with a 14.9% L/D increase at the same angle of attack.

The results show the following trends: i) there was little difference between the cases where the entire top surface was covered and the elevon section only (regions 1 and 2). This indicates that in this design, microfibers are most effective at mitigating flow separation outboard of the wing at high angles of attack. ii) Microfibers perform differently according to the flow regime; At elevated Reynolds numbers, all cases demonstrated comparable L/D advantages at $\alpha = 10^\circ$, although the 70 μm fibers exhibited a marked reduction in their impact at $\alpha = 11^\circ$. In contrast, at lower Reynolds numbers, all cases displayed diminished L/D enhancements at $\alpha = 11^\circ$, followed by an additional decline at higher angles. Analyzing the results for all microfiber cases at $\alpha = 10^\circ$, it is postulated that microfiber pillar size significantly influences aerodynamic performance improvement at the beginning of flow separation, as smaller microfibers offer fewer benefits at higher Re . In the presence of increased turbulence, the 70 μm fibers do not re-energize the boundary layer to the same extent as the 140 μm fibers, owing to the smaller secondary vortices generated and, consequently, the reduced turbulent kinetic energy. On the other hand, in a less turbulent flow, the smaller fibers provide the most significant performance improvement, as they can boost momentum in the external flow without introducing an excessive amount of turbulent kinetic energy.

DOI: ADD DOINUMBER HERE

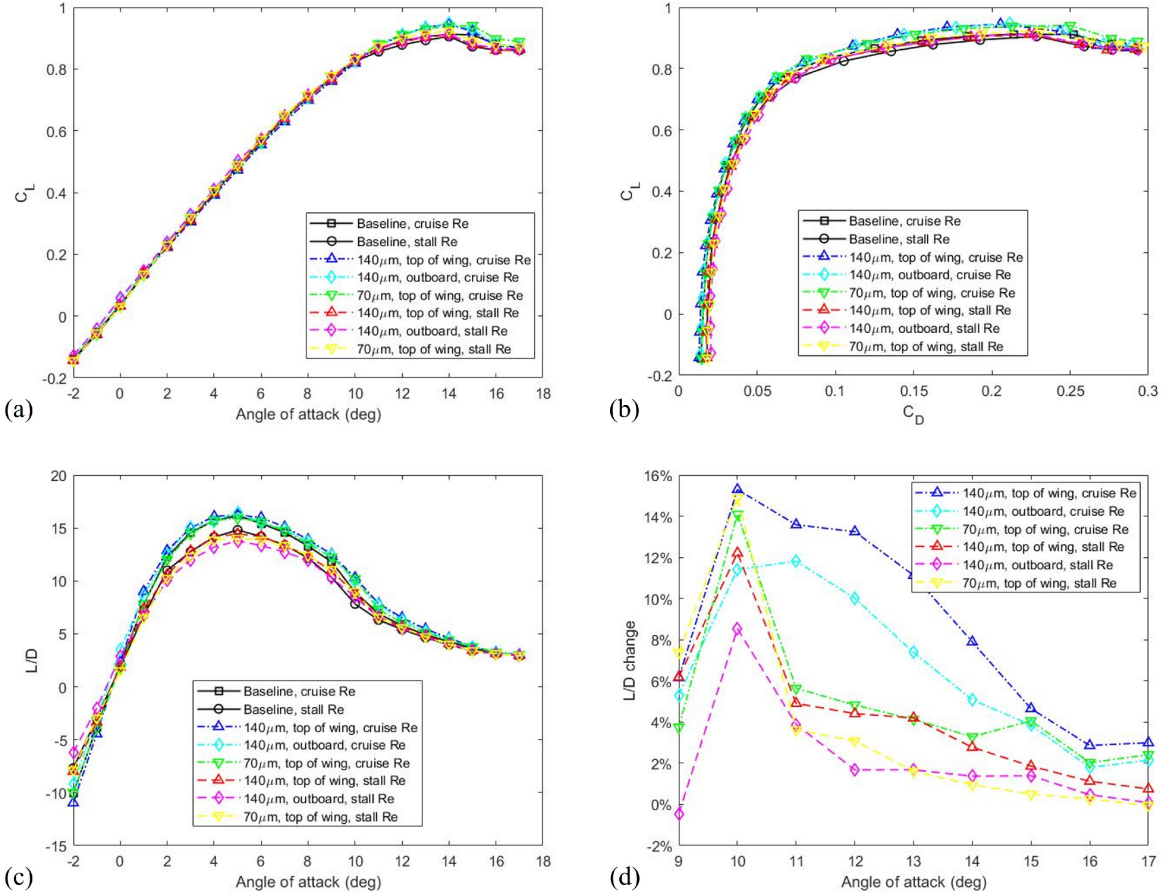


Figure 4: (a) Lift coefficient as a function of angle of attack; (b) Drag polar; (c) Lift-to-drag ratio, L/D ; d) High AoA L/D enhancement.

The control surface performance shown in Figure 5 indicates that changes in pitching moment by use of microfibers on the surface depend on the angle of attack of the aircraft, and at certain conditions the fibers have opposing effects. At $\alpha = 2^\circ$, microfibers covering the top surface of the wing reduced the C_M magnitude by 11.1% for an elevon deflection $\delta_e = 15^\circ$. At medium angle of attack $\alpha = 7^\circ$, the fibers showed negligible effect on control surface pitching performance. For $\alpha = 12^\circ$, the use of fibers revealed to be beneficial to elevon performance, with a maximum increase in C_M magnitude of 15.6% for $\delta_e = 15^\circ$ with the fully-covered top surface, whereas for the partially covered wing, the increase was of 22.4% at same deflection. This behavior exhibits a nonlinear spanwise interplay in the flow between microfiber regions, where supplementing the wing surface with more microfibers becomes counterproductive or less efficient. A comparable effect was observed on a rotor utilizing synthetic jets at transitional Reynolds numbers [31]. In that case, the optimal application of synthetic jets for enhancing the rotor's figure of merit was found in the blade tip area. Activating more synthetic jets towards the central and root sections of the blade demonstrated diminishing returns in rotor thrust, given the extra energy input required for the jets. A distinct parallel between the fixed-wing in this study and the referenced rotor blade lies in the significantly three-dimensional (3D) flow, featuring spanwise movement on both the wing and blade tip regions. The findings indicate that microfibers can serve as an efficient passive flow control method for finite wings with 3D flow and at elevated angles of attack, where preventing stall and maintaining flight control are crucial.

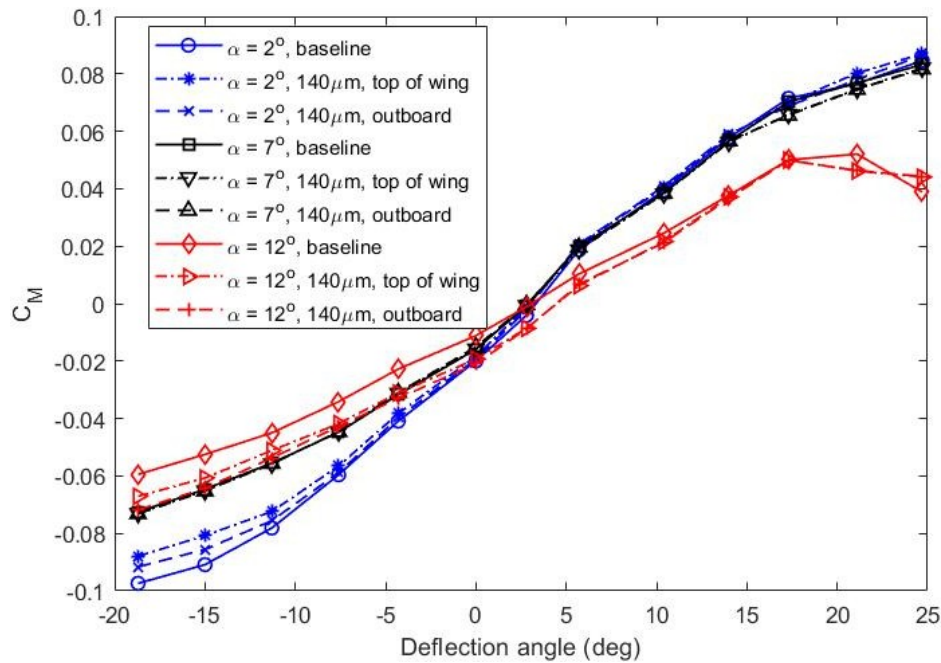


Figure 5: Elevon deflection performance

4. Conclusion

In this work, bio-inspired microfibers were applied to the top suction surface of a small fixed-wing UAV and their effect on aerodynamic performance was studied with wind tunnel experiments. Dependence on flow regime, angle of attack, area of coverage, and fiber height was assessed for lift and drag coefficients, as well as L/D ratio. For a cruise Reynolds number of 3.7×10^5 , $140 \mu\text{m}$ fibers provided the greatest reduction in drag, 24.7% when covering the entire upper surface of the wing. At the stall Reynolds number of 2.1×10^5 , $70 \mu\text{m}$ fibers perform better, reducing the drag by a maximum of 24.2%. It was observed that improvements in performance by use of microfibers are obtained at higher angles of attack, when flow separation is prevalent and where the fibers are able to delay flow separation and restore aerodynamic performance. At lower angles of attack, such as $\alpha = 5^\circ$, the fibers only had marginal effect on aerodynamic efficiency; at cruise Reynolds, L/D was increased by 1.8%, and at stall Reynolds it was reduced by 6.9%. With control surface experiments, fibers covering the elevon and upstream region increased the pitching capability of the aircraft at $\alpha = 12^\circ$, enhancing C_M by 22.4% with a surface deflection of 15° . The results show that there is great potential in applying bio-inspired microfibers to the design of small-scale UAV design, in particular for their benefits at higher angles of attack, or high- α flight which is associated to a highly maneuverable UAV with superior pitch and roll performance. It is posited that a favorable enhancement in the L/D ratio can be attained through meticulous microfiber design, including the optimization of microfiber pillar height, particularly at lower Reynolds numbers. Future work will focus on flow measurement techniques, such as particle image velocimetry, to supplement load cell data and deepen the understanding on microfiber performance.

References

- [1] Raymer, D., *Aircraft Design: A Conceptual Approach*, 5th ed., American Institute of Aeronautics and Astronautics, Reston, VA, 2012, pp. 223 – 225. <https://doi.org/10.2514/4.869112>.
- [2] Lin, J. C., “Review of research on low-profile vortex generators to control boundary-layer separation,” *Progress in Aerospace Sciences*, Vol. 38, No. 4, 2002, pp. 389–420. [https://doi.org/https://doi.org/10.1016/S0376-0421\(02\)00010-6](https://doi.org/https://doi.org/10.1016/S0376-0421(02)00010-6).
- [3] Lissaman, P., “Low-Reynolds-number airfoils,” *Annual review of fluid mechanics*, Vol. 15, No. 1, 1983, pp. 223–239.

DOI: ADD DOINUMBER HERE

- [4] Zhen, T. K., Zubair, M., and Ahmad, K. A., “Experimental and Numerical Investigation of the Effects of Passive Vortex Generators on Aludra UAV Performance,” *Chinese Journal of Aeronautics*, Vol. 24, No. 5, 2011, pp. 577–583.
- [5] Zhu, C., Chen, J., Wu, J., and Wang, T., “Dynamic stall control of the wind turbine airfoil via single-row and double-row passive vortex generators,” *Energy*, Vol. 189, 2019, p. 116272. <https://doi.org/https://doi.org/10.1016/j.energy.2019.116272>.
- [6] Zhou, Y., and Wang, Z. J., “Effects of Surface Roughness on Separated and Transitional Flows over a Wing,” *AIAA Journal*, Vol. 50, No. 3, 2012, pp. 593–609. <https://doi.org/10.2514/1.J051237>.
- [7] Ben-Gida, H., Stefanini, J., Stalnov, O., and Gurka, R., “Application of passive flow control techniques to attenuate the unsteady near wake of airborne turrets in subsonic flow,” *Aerospace Science and Technology*, Vol. 119, 2021, p. 107129. [https://doi.org/ https://doi.org/10.1016/j.ast.2021.107129](https://doi.org/https://doi.org/10.1016/j.ast.2021.107129).
- [8] Serdar GENÇ, M., KOCA, K., and AÇIKEL, H. H., “Investigation of pre-stall flow control on wind turbine blade airfoil using roughness element,” *Energy*, Vol. 176, 2019, pp. 320–334. <https://doi.org/https://doi.org/10.1016/j.energy.2019.03.179>.
- [9] Winzen, A., Klaas, M., and Schröder, W., “High-Speed Particle Image Velocimetry and Force Measurements of Bio-Inspired Surfaces,” *Journal of Aircraft*, Vol. 52, No. 2, 2015, pp. 471–485. <https://doi.org/10.2514/1.C032742>,
- [10] Hu, H., and Tamai, M., “Bioinspired Corrugated Airfoil at Low Reynolds Numbers,” *Journal of Aircraft*, Vol. 45, No. 6, 2008, pp. 2068–2077. <https://doi.org/10.2514/1.37173>.
- [11] Bie, D., Li, D., Xiang, J., Li, H., Kan, Z., and Sun, Y., “Design, aerodynamic analysis and test flight of a bat-inspired tailless flapping wing unmanned aerial vehicle,” *Aerospace Science and Technology*, Vol. 112, 2021, p. 106557.
- [12] Sui, T., Zou, T., and Riskin, D., “Optimum Design of a Novel Bio-Inspired Bat Robot,” *IEEE Robotics and Automation Letters*, Vol. 7, No. 2, 2022, pp. 3419–3426. <https://doi.org/10.1109/LRA.2022.3146536>.
- [13] Fish, F. E., *Biomimetics and the Application of the Leading-Edge Tubercles of the Humpback Whale Flipper*, Springer International Publishing, Cham, 2020, pp. 1–39. https://doi.org/10.1007/978-3-030-23792-9_1.
- [14] Guerreiro, J. L. E., and Sousa, J. M. M., “Low-Reynolds-Number Effects in Passive Stall Control Using Sinusoidal Leading Edges,” *AIAA Journal*, Vol. 50, No. 2, 2012, pp. 461–469. <https://doi.org/10.2514/1.J051235>, URL <https://doi.org/10.2514/1.J051235>.
- [15] Rose, B., and Vt, G., “Aerodynamics with state-of-the-art bioinspired technology: Tubercles of humpback whale,” *Proceedings of the Institution of Mechanical Engineers Part G Journal of Aerospace Engineering*, Vol. 235, 2021. <https://doi.org/10.1177/09544100211001501>.
- [16] Chowdhury, S., and Maldonado, V., *Experimental and Computational Investigation of Passive Surface Flow Control for Aerodynamic Efficiency*, <https://doi.org/10.2514/6.2017-4120>.
- [17] Dou, Z., Wang, J., and Chen, D., “Bionic research on fish scales for drag reduction,” *Journal of Bionic Engineering*, Vol. 9, No. 4, 2012, pp. 457–464.
- [18] Chen, D., Chen, H., and Cui, X., “Dual-coupling drag reduction inspired by tuna skin: Fan-shaped imbricated fish scale composited with flexible coating,” *AIP Advances*, Vol. 12, No. 3, 2022, p. 035218. <https://doi.org/10.1063/5.0066195>.
- [19] Mosghani, M. M., Alidoostan, M. A., and Binesh, A., “Numerical analysis of drag reduction of fish scales inspired Ctenoid-shape microstructured surfaces,” *Chemical Engineering Communications*, Vol. 0, No. 0, 2021, pp. 1–16. <https://doi.org/10.1080/00986445.2021.1992398>.

DOI: ADD DOINUMBER HERE

- [20] Muthuramalingam, M., Puckert, D. K., Rist, U., and Bruecker, C., “Transition delay using biomimetic fish scale arrays,” *Scientific Reports*, Vol. 10, No. 1, 2020, p. 14534. <https://doi.org/10.1038/s41598-020-71434-8>.
- [21] Bixler, G. D., and Bhushan, B., “Fluid Drag Reduction with Shark-Skin Riblet Inspired Microstructured Surfaces,” *Advanced Functional Materials*, Vol. 23, No. 36, 2013, pp. 4507–4528.
- [22] Friedmann, E., Portl, J., and Richter, T., *A Study of Shark Skin and Its Drag Reducing Mechanism*, Springer Berlin Heidelberg, Berlin, Heidelberg, 2010, pp. 271–285. https://doi.org/10.1007/978-3-642-04068-9_16, URL https://doi.org/10.1007/978-3-642-04068-9_16.
- [23] Domel, A. G., Domel, G., Weaver, J. C., Saadat, M., Bertoldi, K., and Lauder, G. V., “Hydrodynamic properties of biomimetic shark skin: effect of denticle size and swimming speed,” *Bioinspiration & Biomimetics*, Vol. 13, No. 5, 2018, p. 056014. <https://doi.org/10.1088/1748-3190/aad418>.
- [24] Afroz, F., Lang, A., Habegger, M. L., Motta, P., and Hueter, R., “Experimental study of laminar and turbulent boundary layer separation control of shark skin,” *Bioinspiration & Biomimetics*, Vol. 12, No. 1, 2016, p. 016009. <https://doi.org/10.1088/1748-3190/12/1/016009>.
- [25] Yu, C., Liu, M., Zhang, C., Yan, H., Zhang, M., Wu, Q., Liu, M., and Jiang, L., “Bio-inspired drag reduction: From nature organisms to artificial functional surfaces,” *Giant*, Vol. 2, 2020, p. 100017. <https://doi.org/https://doi.org/10.1016/j.giant.2020.100017>.
- [26] Lang, A. W., Motta, P., Hidalgo, P., and Westcott, M., “Bristled shark skin: a microgeometry for boundary layer control?” *Bioinspiration Biomimetics*, Vol. 3, No. 4, 2008, p. 046005. <https://doi.org/10.1088/1748-3182/3/4/046005>.
- [27] Evans, H. B., Hamed, A. M., Gorumlu, S., Doosttalab, A., Aksak, B., Chamorro, L. P., and Castillo, L., “Engineered bio-inspired coating for passive flow control,” *Proceedings of the National Academy of Sciences*, Vol. 115, No. 6, 2018, pp. 1210–1214. <https://doi.org/10.1073/pnas.1715567115>.
- [28] Doosttalab, A., Dharmarathne, S., Bocanegra Evans, H., Hamed, A. M., Gorumlu, S., Aksak, B., Chamorro, L. P., Tutkun, M., and Castillo, L., “Flow modulation by a mushroom-like coating around the separation region of a wind-turbine airfoil section,” *Journal of Renewable and Sustainable Energy*, Vol. 10, No. 4, 2018, p. 043305.
- [29] Maldonado, V., Santos, D., Wilt, M., Ramirez, D., Shoemaker, J., Ayele, W., Beeson, B., Lisby, B., Zamora, J., and Antu, C., ‘Switchblade’: *Wide-Mission Performance Design of a Multi-Variant Unmanned Aerial System*, 2021, <https://doi.org/10.2514/6.2021-0213>.
- [30] Maldonado, V., Peralta, N., Gorumlu, S., and Ayele, W., “On the figure of merit and streamwise flow of a propulsive rotor with synthetic jets,” *Aerospace Science and Technology*, Vol. 113, 2021. <https://doi.org/10.1016/j.ast.2021.106712>, URL <https://doi.org/10.1016/j.ast.2021.106712>.